Journal Pre-proofs

Effect of drug load on the aerosolisation propensity of binary adhesive mixtures for inhalation

Anna Simonsson, Tobias Bramer, Alex Wimbush, Göran Alderborn

PII: S0378-5173(24)00356-9
DOI: https://doi.org/10.1016/j.ijpharm.2024.124122
Reference: IJP 124122

To appear in: *International Journal of Pharmaceutics*

Received Date: 16 January 2024
Revised Date: 12 April 2024
Accepted Date: 12 April 2024

Please cite this article as: A. Simonsson, T. Bramer, A. Wimbush, G. Alderborn, Effect of drug load on the aerosolisation propensity of binary adhesive mixtures for inhalation, *International Journal of Pharmaceutics* (2024), doi: https://doi.org/10.1016/j.ijpharm.2024.124122

April 12, 2024

Effect of drug load on the aerosolisation propensity of binary adhesive mixtures for inhalation

Anna Simonsson[1,*], Tobias Bramer[2], Alex Wimbush[2] and Göran Alderborn[1]

[1]Department of Pharmaceutical Biosciences and the Swedish Drug Delivery Center (SweDeliver), Uppsala University, Box 591, SE-751 24 Uppsala, Sweden

[2]Inhalation Product Development, Pharmaceutical Technology & Development, AstraZeneca Gothenburg, Sweden

*Contact details for corresponding author:
Department of Pharmaceutical Biosciences, Uppsala University, Box 591, SE-751 24 Uppsala, Sweden. Phone: +46 18 4714473. E-mail: anna.simonsson@uu.se.

CRediT authorship contribution statement:

Anna Simonsson
Conceptualisation, Methodology, Investigation, Formal analysis, Validation, Writing – Original draft, review and editing

Tobias Bramer
Resources, Supervision, Writing – Review and editing

Alex Wimbush
Resources, Supervision, Writing – Review and editing

Göran Alderborn
Conceptualisation, Methodology, Resources, Funding acquisition, Supervision, Writing – Original Draft, Review and editing

Declaration of competing interest

The study is financially supported by AstraZeneca, and TB and AW are employees at AstraZeneca Gothenburg, Sweden. AS and GA have no competing interests to declare.

Abstract

The aim of this study was to investigate how the propensity for aerosolisation in binary adhesive mixtures was affected by the drug load, and to determine whether these findings could be linked to different blend states. Binary blends of two different lactose carriers, each with varying size and morphology, were prepared together with budesonide. *In vitro* aerosolisation studies were conducted at four different pressure drops, ranging from 0.5 to 4 kPa, utilising a Next Generation Impactor. Several dispersion parameters were derived from the relationship between the quantity of dispersed API and the pressure drop. The evolution of the parameters with drug load was complex, especially at low drug loads. While similar responses were observed for both carriers, the range of drug load that could be used varied significantly. The choice of carrier not only influenced the capacity for drug loading but also affected the spatial distribution of the API within the mixture, which, in turn, affected its aerosolisation propensity. Thus, the drug dispersion process could be linked to different configurations of the lactose carrier and budesonide in the blends, i.e. blend states. In conclusion, the study suggests that the concept of blend states can provide an explanation for the complex dispersion process observed in adhesive blends.

Keywords: Carrier size and morphology, Drug load, Blend state, Fine particle fraction, Dispersibility, Rate of dispersion

1. Introduction

A common dosage form for pulmonary delivery is the inhalation powder (Metha, 2018) which generally fall into two categories: carrier-based adhesive blends or carrier-free powders (soft agglomerates and non-cohesive powders). Carrier-based mixtures typically comprise lactose carrier particles to which micronised particles of an active pharmaceutical ingredient (API) adhere. A single carrier particle together with a layer of adsorbed API particles (the adhesion layer) is hereinafter referred to as an adhesion unit. An adhesive mixture consists of a collection of adhesion units, together with a population of free API fines, i.e. API particles that are not attached to a carrier particle. During inhalation, the API particles are supposed to detach from the carrier particles, a process that depends on a variety of factors, including the adhesive and cohesive bindings within the mixture, particle size, surface morphology and the type of inhalation device used (Grasmeijer et al., 2015; Jones and Buckton, 2016; Nguyen et al., 2018; Rudén et al., 2018., Zellnitz et al., 2019; Yeung et al., 2019; Farizhandi et al., 2019). One limitation in the use of adhesive mixtures is the upper dose limit for a single inhaler actuation, due to the need for a substantial volume of carrier particles in the powder. Historically, doses of API used in inhalation powders were in the microgram range, typically 6–500 μg (Sibum et al., 2018), with a drug-to-carrier mass ratio of 1:67.5 (1.5%) described as a suitable target drug concentration. However, new medication possibilities have created a need for adhesive mixtures with considerably higher drug loads. Yeung et al. (2018) reported a variation in drug content for 12 carrier-based inhalation powders, varying from 12 μg to 5 mg. The latter had a drug-to-carrier ratio corresponding to 20% w/w of the drug. The definition of a high dose and, hence, the boundary line between low and high doses of drugs administered by inhalation is not clearly defined in the literature. Sibum et al. (2018) proposed that doses up to 2.5 mg are considered low doses, while doses above 2.5 mg are viewed as high doses. This distinction between low and high doses stems from two key assumptions: First, that 2.5 mg represents an approximate upper dose limit for which an adhesive mixture can be used in an inhalation powder and second, that a practical maximum for drug concentration in an adhesive mixture is 10% (with a drug-to-carrier ratio of 1:9). Thus, although adhesive mixtures are, in practice, restricted to low and intermediate doses, the range of drug load can vary significantly, and consequently also the drug concentration (drug load) in the mixture.

The drug concentration in an adhesive mixture, in combination with the particle and surface properties of both the drug and the carrier, will affect the spatial distribution of the drug particles within the blend. Accordingly, efforts to generalise the structural changes that an adhesive blend undergoes with an increased amount of drug fines in terms of consecutive series of stages have been presented in the literature (Young et al., 2011; Rudén et al., 2018 and 2019). Moreover, it is proposed that the structure of the mixture (Young et al., 2011) or its blend state (Rudén et al., 2021) determines the extent to which drug particles disperse as inhalable particles during actuation of a dry powder inhaler (DPI). Thus, the concept of blend state may be useful in providing an understanding of the variables that impact the aerosolisation propensity of adhesive mixtures, warranting further investigation.

The aim of this study was to investigate the relationship between drug load, blend state and the aerosolisation propensity of a series of adhesive mixtures. We specifically ask if the drug load dependent variation in aerosolisation propensity could be linked to the blend state of the mixtures, i.e. if the underlying cause for the variation in aerosolisation propensity is a change in the

localisation of attached drug particles and the microstructure of the adhesive layer. To do so, a series of binary adhesive mixtures containing different drug (budesonide) loads were prepared, using two lactose carriers of different size and morphology.

2. Materials and methods

2.1. Materials

Micronised Budesonide was provided by AstraZeneca Gothenburg (Sweden) and used as the active pharmaceutical ingredient (API). Inhalac 70 and Inhalac 230 were provided by Meggle (Germany) and used as carriers. Particle characteristics of these powders are presented in Table 1. Furthermore, Tween 80 (Merck KGaA, France) was used as the wetting agent.

LC grade methanol and acetonitrile (VWR International, Fontenay-sous-Bois, France) were used for the UPLC analysis, together with MiliQ water (produced using Purelab Flex ELGA, LabWater, United Kingdom). Fluocinolone acetonide, used as an internal standard (Sigma Aldrich, USA), was diluted in Ethanol (Solveco, Sweden). The phosphate buffer was prepared from sodium dihydrogen phosphate and orthophosphoric acid (both from Sigma Aldrich, Switzerland), as well as MilliQ water. Additionally, the NGI coating agents (Brij 35 and glycerol) were acquired from Sigma Aldrich (Ontario, Canada and Germany, respectively).

2.2. Particle characterisation

The particle size was determined by laser diffractometry (Beckman Coulter LS 230, small, volume module plus, USA). Prior to performing the measurements, the carrier particles were suspended in isopropanol (Merck KGaA, Darmstadt, Germany), while the API particles were suspended in water with 0.1 w/w% Tween 80 ((Merck KGaA, France). All reported values represent the mean of the three measurements. The span was calculated according to the following equation: $Span = \frac{D_{90}-D_{10}}{D_{50}}$ (1)

The apparent particle density was determined using helium pycnometry (AccuPyc 1330, Micromeritics Instruments, Norcross, USA). All reported values represent the mean of five consecutive measurements.

The specific surface area of both the drug and carrier particles was determined by air permeametry, using a transient Blaine permeameter (Alderborn et al., 1985) for the API and a steady-state air permeameter for the carrier particles (Eriksson et al., 1993). For the API particles, the volume-specific surface area was calculated using the Kozeny-Carman equation corrected for slip-flow, as described by Alderborn et al. (1985), using an aspect factor of 5. For the carrier particles, the volume-specific surface area was calculated using the Kozeny-Carman equation, using an aspect factor of 6, as proposed by Eriksson et al. (1993). All reported values represent the mean of the three measurements.

2.3. Preparation of adhesive mixtures

The API and carrier powders were mixed in a Turbula 2F2 mixer (Willy A. Bachofen AG, Switzerland) operated at 46 rpm for 1 hour. Prior to mixing, API particles were sieved through a 750 µm sieve to remove large agglomerates. In all mixtures, 50 grams of carrier were used, while the quantity of API was adjusted in order to get a series of blend concentrations (Table 2). A 250

ml glass jar served as the mixing container into which the powders were placed, following a "sandwich method" approach. Thus, the carrier and API were placed in layers into the jar in three steps, with the API in the middle layer. Approximately half of the container was filled with the powders before commencing the mixing.

The surface coverage ratio (SCR) of the mixtures, which theoretically indicates the extent to which the carrier surface is covered with fines, was calculated as follows (Rudén et al., 2018; Rudén et al., 2019):

$$SCR = \frac{\alpha m_f S_{w,f}}{m_c S_{w,c}} \qquad (2)$$

where m_f and m_c represent the masses of the fines and the carrier particles, respectively, and $S_{w,f}$ and $S_{w,c}$ represent the weight-specific surface areas of the fines and the carrier particles. α was set to $1/\pi$, assuming that spherical particles cannot cover the surface completely. A SCR of unity represents, theoretically, a situation where the carrier surface is completely covered by a mono-layer of drug particles.

All powders and mixtures were stored in a climate-controlled room, at a temperature of 21–24°C and a relative humidity of 30–34%, for a minimum of 24 hours.

2.4. Assessment of mixture homogeneity

Mixture homogeneity was assessed by drawing 10 samples of 15–20 mg from every mixture, and their API content was subsequently determined by scooping. All samples were retrieved from the same glass vial as used during the powder mixing. However, they were drawn from different positions within the mixture (horizontally and vertically), and approximately the same positions were used for all the mixtures.

The samples were dissolved in 20 ml of internal standard solution, comprising fluocinolone acetonide in ethanol (95%) at a concentration of 40 mg/L, while being agitated on a shaking table. Thereafter, 0.5 ml of the API solution was drawn from each sample and placed into separate LC vials, together with 0.8 ml phosphate buffer solution (pH 3.2), aiming to improve the resolution of the peaks during the UPLC analysis. The amount of API in each sample was determined using a Waters Acquity UPLC system (Waters Corp, Milford, USA). The mobile phases consisted of two separate phases: "A" (water and 0.03% trifluoracetic acid) and "B" (acetonitrile and 0.03% trifluoracetic acid). The composition of the mobile phases flowing through the column was 65% A and 35% B. The amount of API was calculated by using a calibration curve, with a correlation coefficient R^2 of at least 0.999. The UV wavelength was set at 254 ± 10 nm.

The same analytical procedure, as described here, was also used to determine the quantity of API deposited in the impactor cups during the aerosolisation study (see section 2.6).

2.5. Particle imaging

Scanning electron microscopy (SEM) images were captured using a Zeiss 1530 (Carl Zeiss GmbH, Jena, Germany) microscope, operating at an acceleration voltage of 2.5 kV. The images were taken using an InLens detector at 5–10kx magnification. Before taking the images, samples were coated with gold/platinum.

In order to illustrate the presence of self-agglomerates of API formed at high drug loads, light microscope images were obtained, using a Zeiss SteREO Dis-covery.V8 (Carl Zeiss GmBH, Oberkochen, Germany) at 1× magnification.

2.6. Assessment of mixture aerosolisation behaviour

Dispersion experiments were performed using a Next Generation Impactor (NGI) (Copely Scientific, UK), equipped with a Screenhaler device and a Turbuhaler mouthpiece (Thalberg et al., 2016). Pressure drops of 0.5, 1, 2 and 4 kPa were applied across the impactor, and the suction time was adjusted using a Triggbox model III (AB FIA, Lund, Sweden) to correspond to a 4 L suction volume. A solution containing ethanol (51%), Brij 35 (15%) and Glycerol (34%) (Rudén et al., 2022) was prepared, which was then used to coat the NGI cups, aiming to reduce the occurrence of particle bouncing between the stages.

Prior to each individual experiment, the inhaler device was loaded with an API dose ranging from 15–17 mg. In order to reach quantifiable amounts of the API during the chemical analysis, several actuations were used. The limit of quantification was set to 5 µg.

Thereafter, 20 ml of the internal standard solution was added to each NGI cup, the throat and the pre-separator (see section 2.4). The NGI cups were agitated for 20 minutes using a standard laboratory shaking table (Heidolph instruments, Germany), while the throat and pre-separator were also agitated for 20 minutes using a sample preparation unit (Copely Scientific, UK). When the API had dissolved in the internal standard solution, 0.5 ml of each sample was transferred to individual vials. Then, 0.8 ml of phosphate buffer solution (pH 3.2) was added to each vial.

The emitted dose (ED) was calculated by adding the sum of the API weights collected in all stages of the impactor (1-MOC), including the throat and pre-separator. The fine particle fraction (FPF) was calculated as the fine particle dose (FPD) divided by the emitted dose. The FPD is here defined as the mass of API particles with an aerodynamic particle diameter equal to or below 5 µm.

The masses of API deposited in the NGI impactor body in stages 2 to 7 and in the MOC cups were used to construct a cumulative aerodynamic particle diameter distribution. The API mass deposited in each cup was plotted as a function of the corresponding aerodynamic cut-off particle diameter. From the cumulative distribution, the mass median aerodynamic diameter (MMAD) was determined as the diameter corresponding to a cumulative mass fraction of 0.5, obtained by linear interpolation within a range defined by the nearest upper and lower diameters.

2.7. Calculation of dispersion parameters

As indicators of the aerosolisation propensity of the mixtures, a series of dispersion parameters were calculated based on the relationships between the degree of dispersion and pressure drop (ΔP).

From the relationship between the FPF and pressure drop, two dispersion parameters were calculated, representing the maximum degree of dispersion and the rate of dispersion, respectively, by the following equation (Elsayed and Shalash 2018):

$$FPF = FPF_{\max,}\,(1 - \exp[-k_{d,}\,\Delta P]) \qquad (3)$$

where FPF_{max} represents an indication of the FPF at an infinite pressure drop and k_d denotes the dispersion rate constant, indicating the rate of FPF change concerning the pressure drop. In order to calculate $k_{d,}$ a curve fitting technique was used, i.e. a starting value for FPF_{max} was used, after which the best curve fit was obtained through iteration. From this curve, the two parameters were determined for each mixture. The starting value for iteration was an estimation of $FPF_{max,}$ which was obtained by fitting the experimental FPF-ΔP relationships to the following expression:

$$\frac{\Delta P}{FPF} = \frac{1}{FPF_{\max}}\Delta P + \frac{\Delta P_{\text{half}}}{FPF_{\max}} \qquad (4)$$

where ΔP_{half} represents the pressure drop that is required to achieve 0.5 $FPF_{max.}$

The pressure drop sensitivity was calculated in two ways, using FPF and MMAD data, respectively, in the following ways:

$$\frac{FPF_{\Delta P\ 4\ kPa} - FPF_{\Delta P\ 0.5\ kPa}}{FPF_{\Delta P\ 0.5\ kPa}} \qquad (5)$$

and

$$\frac{MMAD_{\Delta P\ 0.5\ kPa} - MMAD_{\Delta P\ 4\ kPa}}{MMAD_{\Delta P\ 4\ kPa}} \qquad (6)$$

Another indication of the maximum degree of dispersion that could be obtained, referred to as the minimum achievable MMAD ($MMAD_{min}$), was calculated from the relationship between the inverted MMAD (1/MMAD) and the pressure drop similar to equation 4, as follows:

$$\frac{\Delta P}{\frac{1}{MMAD}} = MMAD_{min} * \Delta P + MMAD_{min} * \Delta P_{half} \qquad (7)$$

3. Results

3.1. Particle dimensions

The budesonide microparticles had a median particle diameter of 2.1 μm and a specific surface area of about 4.5 m^2/g (Table 1). The particle diameter distribution (under the influence of pressure drop, during the aerosolisation experiments) was asymmetrical around the median diameter (Figure 1). Hence, the diameter spread was considerably higher for particles larger than the median, i.e. in the range of 2 to about 8 μm, compared to those below the median.

Due to the small size and cohesive nature of the primary API particles they formed irregular agglomerates (as shown in Figure 2). The shape of the primary API microparticles (Figure 2) varied from relatively regular in shape with a rounded character to slightly elongated. The surface of the API microparticles were relatively smooth.

Inhalac 70 had a median particle diameter approximately 2.5 times larger than Inhalac 230 and also had a significantly larger span, i.e. a broader size distribution (Table 1). The geometrical shape of both carrier particles (Figure 2) was similar, with the tomahawk shape typical of crystalline lactose particles (Zeng et al., 2000), with low surface roughness. However, some of the carrier particles were irregular, with surface protrusions and sharp corners, i.e. showing a marked surface roughness. The irregular carrier particles seemed to be more prevalent in Inhalac 70 compared to Inhalac 230.

3.2. Blend homogeneity and appearance

Since the carrier particles had different external surface areas (Table 1), the Surface Coverage Ratio (SCR) was used to prepare mixtures of potentially comparable blend structures. However, the same SCR gave different drug concentrations for each carrier. Since a considerably higher drug load could be used for Inhalac 70 compared to Inhalac 230, before a population of free API particles appeared as self-agglomerates (i.e. Inhalac 70 had a higher loading capacity), more mixtures were prepared for the larger carrier.

The variation in blend homogeneity (Table 2) mostly remained below or close to 5% for mixtures of both carriers, i.e. a threshold considered as the maximum acceptable variation for inhalation powders (Nguyen et al., 2015). The variations in homogeneity were markedly higher at low drug loads (Inhalac 230) and high drug loads (Inhalac 70 and 230). The increased variation could be due to local variations in the adhesion layer structure at low drug load and the existence of free API self-agglomerates at high drug loads. For about half of the mixtures, the measured drug load was higher than the corresponding nominal values and for the other half, lower values corresponding to a percentage deviation from the nominal value of up to 13% (with the exception of the Inhalac 70 mixture of the highest drug load). These deviations are probably mainly due to stochastic variations rather than systematic effects.

Figure 3 shows the appearance of selected mixtures with different drug concentrations for both carriers. The elevated drug concentrations led to increased drug adherence to the carrier surface. As visually judged from the SEM images of the Inhalac 70 mixtures, an increase in drug concentration gradually resulted in an increased surface coverage of the carrier particles and a

thicker drug layer, but which also became more uneven at the highest drug concentrations. The SEM images of the Inhalac 230 mixtures indicated the formation of a more heterogeneous distribution of drug particles over the carrier surface with small lumps of drug particles.

Thus, this evolution in the adhesive layer structure seemed to differ between the two carriers. Nonetheless, for both carriers, self-agglomerates of the drug appeared at the highest drug loads, as illustrated in Figure 4 through images obtained by light microscopy.

3.3. Blend dispersion

3.3.1. Distribution of emitted dose between the main impactor parts

Elevated drug concentrations typically increased the emitted dose (ED) (Figure 5). Generally, the ED remained lower than the nominal dose, and the retained dose (RD) increased with increased drugload (Figure 5), i.e. the difference between the nominal and emitted doses, increased with drug load.

At the highest dose strengths, greater variability was observed among the replicates, leading to a decreased RD. The pressure drop had a limited effect on the emitted dose, but the ED had a tendency to increase with pressure drop, although this was not consistent for all mixtures.

For Inhalac, 70 the lowest ED fractions were observed in the throat, while the highest fractions were found in the pre-separator, with the intermediate ED fractions in the impactor stages (Figure 6). For Inhalac, 230 the gross distribution of the emitted dose among the main impactor parts was similar to that of Inhalac 70, albeit more uniform (Figure 6).

The effect of the drug load on the fraction of ED deposited in the parts of the impactor showed similar responses at all pressure drops. For Inhalac 70, the response was characterised by an initial increase (pre-separator) or decrease in deposition (throat and impactor stages) until a maximum or minimum was reached at around 4% of the drug load (corresponding to a SCR of 2) and thereafter, the deposition either decreased or increased (Figure 6). For Inhalac 230 a more consistent change in the deposition response with drug load was obtained, where the dose deposited in the throat increased with drug load, while in the pre-separator, it decreased. In the NGI stages, a variable deposition with drug load occurred without an obvious trend (Figure 6).

For Inhalac 70 an increased pressure drop tended to decrease the drug deposition in the pre-separator and consequently increase the deposition in the throat and the NGI stages (Figure 6). For Inhalac 230, there was no significant effect of pressure drop on the fraction of ED deposited in the respective parts of the impactor (Figure 6).

3.3.2. Distribution of fine particles between the impactor stages

The distribution of particles in the different stages of the impactor was generally asymmetrical around the median diameter. Relevant examples of cumulative distributions of the aerodynamic diameter, illustrating this skewness, are shown in Figure 1. From the distributions of particles

within the impactor stages, three measures for fine particles were calculated, i.e. the fine particle dose (FPD), fine particle fraction (FPF) and the mass median aerodynamic diameter (MMAD). For this study, we used a common definition of a fine particle, i.e. a particle having a maximal aerodynamic diameter of 5 μm.

Regarding the effect of the pressure drop on the derived fine particle measures, similar trends were observed for both carrier mixtures. An increase in pressure drop resulted in elevated FPD and FPF, while MMAD decreased (Figure 7). The decrease in MMAD can mainly be explained by a decrease in the proportion of particles with larger aerodynamic diameters and a corresponding increase in the proportion of particles with small aerodynamic diameters, resulting in a more narrow, less skewed size distribution (Figure 1). The effect of pressure drop on the skewness of the aerodynamic diameter distribution became more pronounced at high drug loads, i.e. an increased drug load increased the pressure drop sensitivity of the mixtures.

Regarding the effect of drug load on FPD, an increase in drug load resulted in a gradual increase in FPD across all pressure drops for both carriers but the relationships tended to oscillate around a linear progression. This oscillation tended to become more pronounced with higher pressure drops (Figure 7).
It is noteworthy that for Inhalac 70, difference in FPD observed at the two highest drug loads (i.e. the drug load at which the API self-agglomerates appeared), is considered to be insignificant.

The impact of drug load on FPF and MMAD revealed that the relationships could generally be described as having a complicated evolution. In mixtures with Inhalac 70 at the lowest pressure drop, FPF initially decreased with increased drug load, but tended to stabilise at approximately 5% budesonide. At higher pressure drops, FPF, at first, decreased with drug load, followed by an increase up to 1.5% budesonide. Thereafter, FPF decreased more gradually to a drug load of 4–5%, then increased again before, finally, stabilising. Thus, for most pressure drops, the FPF-drug load relationships could be described as displaying a wave-like response with peaks occurring at different drug loads. The MMAD-drug load relationships exhibited a similar wave-like response (Figure 7).

For Inhalac 230, the FPF-drug load relationship displayed a similar wave-like progression, albeit occurring over a much more limited drug load range. The MMAD-drug load relationship followed the same progression at the two higher pressure drops, but it showed a simpler relationship with a gradual decrease in MMAD with drug load at the two lower pressure drops (Figure 7).

Not unexpectedly, an increased pressure drop generally shifted the FPF-drug load relationship towards higher FPF values and shifted the MMAD-drug load relationship towards lower MMAD values (Buttini et al., 2016).

3.4.Dispersion parameters

The effect of drug load on the evolution of the dispersibility parameters (FPF_{max} and $MMAD_{min}$) is presented in Figure 9. In the figure, the proposed blend states of the mixtures are indicated, as discussed further below. Generally, mixtures of Inhalac 230 gave a somewhat higher FPF_{max} and $MMAD_{min}$ values compared to the Inhalac 70 mixtures. Thus, the relative amount of fine particles generated from the Inhalac 230 mixtures was higher, but these fine particles were slightly larger compared to those from the Inhalac 70 mixtures. Analysing the effect of drug load on the dispersion parameters, the FPF_{max} vs drug load and $MMAD_{min}$ vs drug load relationships displayed a wave-like character. The drug load - FPF_{max} relationships were characterised by two peaks (at maximum drug load and at around 2%) and two valleys at the lowest drug load and at around 5%, i.e. the peaks and valleys occurred approximately at similar drug loads for both carriers.

The drug load - $MMAD_{min}$ relationships showed a similar progression with peaks and valleys at similar drug loads, with Inhalac 70 demonstrating an overall trend towards lower $MMAD_{min}$ with increasing drug load.

In Figure 10, two indications of the pressure drop sensitivity of the mixtures, one based on FPF (left graph) and one based on MMAD (right graph), are presented in relation to drug load. For both measures, the relationships were complex but showed similar wave-like progressions as the dispersion parameters. For Inhalac 70, the overall trend indicated that increased drug load increased the pressure drop sensitivity (see also Figure 1). The Inhalac 230 mixtures showed a similar progression of the relationship but with more pronounced variations and a tendency towards a slightly lower pressure drop sensitivity.

For Inhalac 70, the dispersion rate constant (k_d) decreased gradually with increased drug load in a non-linear way (Figure 11). At low drug loads, there was a fast reduction in k_d with drug load, followed by a considerably slower change. For Inhalac 230, however, a more complex relationship was found between k_d and drug load. A fast reduction in dispersion rate occurred with drug load for the three lowest drug concentrations similar to that observed in Inhalac 70, with their relationships nearly overlapping. Thereafter, there was a markedly higher rate constant followed by a lower one.

For Inhalac 70, an inverted relationship was observed between the two dispersion parameters, k_d and FPF_{max} (Figure 11), i.e. a high dispersibility (FPF_{max}) corresponded, in general terms, to a lower dispersion rate (k_d). At the highest drug loads, the dispersibility markedly decreased with dispersion rate but stabilised at the lowest drug concentrations. The relationship, however, did not change uniformly, and a deviation in the trend was seen at intermediate drug loads.

The corresponding k_d vs FPF_{max} relationship is not presented for Inhalac 230 due to the low range of drug loads that could be used for this carrier, resulting in a restricted number of data points evolving in a complex way.

A comparison between Figures 10 and 11 shows that an increased pressure sensitivity corresponds to a reduced dispersion rate.

4. Discussion

4.1. Experimental design

In vitro impactor studies, such as NGI assessment, generate a multitude of data. In order to concentrate the data to the drug dose relevant for *in vivo*, the relative quantity of fine inhalable particles and their median diameter is typically calculated. Here, we used a common definition of fine particles, i.e. particles having a maximal aerodynamic diameter of 5 μm, and we calculated the corresponding fine particle fraction (FPF). In addition, the mass distribution of particle diameters at impactor stages, denoted 2 to 8 (MOC), was used to calculate the mass median aerodynamic diameter (MMAD).

It is common to study aerosolisation of inhalation powders using cascade impactors operated at a single pressure drop over the inhaler (most commonly 4 kPa). However, the flow rate through or pressure drop over the inhaler may be critical for the actual lung dose delivered (Buttini et al., 2016; Clark et al., 2020). Kassinos et al. (2021, p. 131) reported that a variation in pressure drop for some DPIs gave approximately the same FPF, whilst for others, an increase in pressure drop displayed an increase in FPF. It has also been pointed out (Grasmeijer and de Boer, 2014) that it is preferable to investigate the dispersion of inhalation powders at different flow rates in order to fully understand their aerosolisation properties. Thus, although impactors primarily serve as quality control instruments (Kassinos et al., 2021, p. 151), the use of several flow rates will give a broader dataset that can provide greater understanding of the performance of inhalation powders, having a potential clinical relevance. Hence, the pressure drop over the inhaler is used in this study as an experimental variable.

It has been shown that different inhalers respond differently to flow rates (Buttini et al., 2016); thus, the type of inhaler used will likely affect the dispersion metrics obtained. In this study, we used only one inhaler device; hence, the metrics generated are specific to this inhaler's aerosolisation performance. The device used – a Screenhaler – has a simple design, comprising an angled channel (Thalberg et al., 2016), and was therefore convenient and time saving to use during the experiments. Due to the simple design the Screenhaler has a low dispersion capacity and was connected to a Turbohaler mouthpiece, where the latter is designed with spiral shaped channels so that a non-homogenous, high-shear airflow is developed in the mouthpiece (Zhu et al., 2022). It is thus proposed that the use of the mouthpiece increases the intensity of particle-particle and particle-wall collisions, thereby enhancing the de-agglomeration capacity of the inhaler setup. However, it should be noted that the relatively simple construction of the device generates an overall FPF that is considerably lower than what is expected for commercial devices, which can provide FPF values up to 50% (Demoly et al., 2014). Nevertheless, the device has earlier been shown (Rudén et al., 2022) to be able to discriminate between mixtures of different drug load regarding their dispersibility.

The relationship between FPF and the pressure drop over the impactor (ΔP) has been reported to follow a curved response (Rudén et al., 2022; Hertel et al., 2018; Hoppentocht et al., 2014), asymptotically reaching a maximum value. Different mathematical treatments for characterising the relationship between measures of dispersion and ΔP have been reported in the literature, as

summarised by El Sayed and Shalash (2018). These equations are typically modifications or adaptions of other expressions describing different physical phenomena, such as adsorption at interfaces, solid-state transformations and chemical reactions. They suggest that the degree of dispersion increases with ΔP in a curved manner, approaching a maximal degree of dispersion. The FPF or the MMAD is typically used as indications of the degree of dispersion. Here, we used a modified JMAK equation (Eq. 3) based on FPF data, an equation that includes two dispersion parameters, i.e. an end point parameter (FPF_{max}) and a rate parameter (k_d). Conceptually, these parameters can be understood as indications of the inherent propensity of a powder to aerosolise, i.e. the propensity of a blend to generate airborne particles independent of the measurement conditions (Jaffari et al., 2013). Based on the visual assessment of the FPF-ΔP plots, the experimental data aligned well with the theoretical curves.

The drug loads selected for the adhesive mixtures aimed to cover different blend states or mixture structures. Young et al. (2011) identified five consecutive regions describing the evolution in the mixture structure with drug load. With increased drug load, the structure of the adhesive layer changed from a mono-layer to a multilayer and eventually, the carrier surface became saturated where self-agglomerates of API fines emerged. Rudén and colleagues (2018 and 2019) conceptualised the change in the mixture structure with drug load, using a series of consecutive blend states. The starting point for the concept is that the drug particles may exist either as bonded to the carrier surface (i.e. located in an adhesion layer) or as non-bonded to the carrier, typically existing as free agglomerates of only fines. Four blend states were proposed, denoted as S1, S2a, S2b and S3. The drug load at which S3 appears represents the point at which a significant proportion of the drug particle population exists as a non-bonded fraction, while in the other states, drug particles are located within an adhesion layer of evolving volume. On the drug particle scale, variations in the distribution of the particles within the adhesion layer can occur, such as varying packing density and clusters of varying volumes. Images of the adhesive units (Figures 3 and 4) support the finding that an increasing drug load will change their appearance in concordance with the blend state concept. Moreover, these images indicated that the micro-structure of the adhesion layer differed between the two carriers: Inhalac 70 mixtures developed a coherent, relatively smooth multi-particulate adhesion layer, while Inhalac 230 mixtures presented a more heterogenous layer with dispersed micro-agglomerates at the carrier surface.

The mixing condition was chosen to reach a state where the uniformity of the drug dose is high and constant with mixing time. Since a small laboratory mixer was used, a long mixing time (1 hour) had to be used in order to satisfy this aim, a choice that was based upon previously reported data (Nyström and Malmqvist, 1981).

4.2. Deposition in the main impactor parts

For mixtures of both carriers, the largest fraction of the emitted drug dose was deposited in the pre-separator (Figure 6). In an earlier study (Rudén et al., 2022), structures sampled from the pre-separator had an appearance that was similar to the original adhesive units, i.e. carriers with a layer of adhered drug. Consequently, it is proposed that the majority of the drug deposited in the throat and pre-separator might not have been released from the carrier during the actuation of the inhaler and thus bonded to the carrier surface. However, the drug might detach not only as primary

particles, but also as micro-agglomerates. A fraction of these micro-agglomerates could also deposit in the pre-separator.

For Inhalac 70, excluding the highest drug load, the relationship between the fraction of emitted drug dose (ED) deposited in the various impactor stages and the drug load tended to exhibit a U-shaped response (Figure 6). An increase in the pressure drop led to greater deposition of adhesive units in the throat and increased deposition in the impactor due to increased drug detachment from the adhesive units. Hoppentocht et al. (2014) reported that the probability of particles affecting the upper airways increases with flow rate through the inhaler, which is consistent with the findings here of increased deposition in the throat with a higher pressure drop. Hoppentocht et al. (2014) also reported that an increased pressure drop across the inhaler may elevate the FPF, which is also consistent with the findings observed here.

For Inhalac 230 (Figure 6), the impact of the pressure drop on the fraction of ED in the throat and the impactor was smaller compared to Inhalac 70. However, an increased pressure facilitated the dispersion of the adhesive units while tending to reduce deposition in the throat. Thus, Inhalac 230 particles, which are smaller and have a lower mass compared to the Inhalac 70 particles, displayed a reverse trend concerning the effect of pressure drop on their tendency to deposit in the throat. It seems that adhesive units of Inhalac 230 are more prone to follow the airflow further down the impactor.

The aerodynamic diameter of particles deposited in the impactor stages were generally higher than the physical diameter of the particles measured by the light scattering method (Figure 1). Since different measuring principles were used, the diameter distributions are not directly comparable. However, a comparison between the overall shape of the distributions indicates that the fine particles comprised two particle populations: primary drug particles and micro-agglomerates of drug particles that were not fully dispersed during the impactor measurements. Efforts were made to sample and visually assess if such micro-agglomerates of drug particles existed in the impactor, but these attempts did not provide conclusive results.

4.3. Aerosolisation propensity of Inhalac 70

The fine particle dose (FPD) increased gradually with drug load, but not in a linear manner. In contrast, the FPF vs drug load and the MMAD vs drug load relationships did not show a similar gradual increase; rather, it showed wave-like responses (Figure 7). Thus, although FPD may increase with drug load, it may not directly correlate with the FPF.

The relationship between FPF and drug load for most pressure drops was complex but can be considered as consisting of two regions. The first region showed a variable FPF values with drug load, but without a consistent trend towards increased or decreased FPF with drug load. These variations in this region, here described as a wave-like response, occurred up to a theoretical SCR of about 1 and were large enough to be significant. The second region showed a consistent and gradual increase in FPF with drug load, continuing until the saturation level of the adhesive units was reached. The MMAD-drug load relationships showed a similar complex response.
Within the first region, two waves can be discerned before entering region 2: a first short wave followed by a more elongated wave. Thus, the FPF or MMAD vs drug load relationships can be described as consisting of three drug load phases, which is consistent with an earlier proposed

(Thalberg et al., 2012) generalisation of the relationship between drug load and the dispersion performance of adhesive mixtures as consisting of three drug load regions: the dilute region (<2%), intermediate region (2–15%) and high drug load region (>15%). The same type of wave-like progressions in the relationship between fraction of drug detached and increased drug content has also been previously reported (Grasmeijer et al., 2013b) in adhesive mixtures of fluticasone propionate and lactose (Pharmatose 80M).

It has previously been proposed (Young et al., 2011; Rudén et al., 2021 and 2022) that the aerosolisation behaviour of an adhesive mixture may be linked to the structure or the state of its characteristics. Thus, the underlying explanation for the existence of dispersibility phases within the dispersibility-drug load relationship could be attributed to the evolution of different structural states within an adhesive mixture with varying drug loads, i.e. a blend dispersibility-state relationship. Young et al. (2011) proposed that a change in the structural state of the mixture occurs when the direction of the evolution of the FPF vs drug load relationship shifts, i.e. a change from a negative to a positive slope, vice versa or a change from a slope to a plateau. By applying the approach used by Young et al. (2011) in combination with the visual assessments of when the self-agglomerates appeared, the proposed blend states are highlighted within the dispersibility-drug load relationships, as shown in Figure 9. For the Inhalac 70 mixtures, the relationship between FPF_{max} vs drug load (Figure 9) can be divided into three phases, with two phase transitions that could be linked to the proposed blend states in the blend state theory. At low drug loads, i.e. a blend state 1 (S1) situation), an increase in drug load means a decrease in FPF. The same direction of the FPF vs drug load relationship was also proposed by Young et al. (2011) for low drug loads, i.e. the type I region. At a specific drug load, the FPF_{max} increased, proposed to be associated with the formation of blend state 2a (S2a). Thereafter, the FPF_{max} decreased gradually, reaching a valley and then again increased again, which may be explained by a transition from S2a to blend state 2b (S2b). Finally, free-agglomerates formed, resulting in a further change in the FPF_{max} variable, dependent on the pressure drop. The $MMAD_{min}$ also changed with drug load (Figure 9), and similar to $FPF_{max,}$ the overall response can be linked to blend states. Within S1 and S2a, the dominating trend shows a decrease in MMAD with increasing drug load, while in S2b, the MMAD tended to increase with drug load.

Young et al. (2005) reported a U-shaped relationship between FPF and drug load, occurring over a loaded drug dose of approximately 10 to 450 μg. This relationship is, thus, similar to the second dispersibility phase reported here (i.e. blend state 2). In contrast to this study, Young et al. (2005) did not obtain an initial first U-shaped relationship at very low drug loads. The presence or absence of the first phase might be due to a difference in the carrier morphology, affecting the mass fraction of drug particles located in blend state 1.

Zellnitz et al. (2014) studied the aerosolisation of adhesive blends using smooth glass beads as carrier particles, which hence is a carrier for which a blend state 1 mixture, by definition, cannot be formed. They reported that the FPF increased almost in a linear manner with SCR, which is similar to what is found here for Inhalac 70 for the part of the FPF-drug load relationship considered to be a blend state 2b mixture.

The wave-like response may be explained by the hypothesis that the dispersibility of drug particles is controlled by a complex interplay of three factors: their localisation on the carrier surface, their

bonding to the carrier surface and to other neighbouring drug particles, and the mechanism of detachment. At lower drug loads, the drug particles are located within the surface cavities (S1) as predominantly free, separated particles. These particles adhere to the carrier surface by adhesion forces, i.e. drug-carrier bonds, without interference from other bonds. With rising drug concentration, the surface concentration of the drug will increase and eventually reach a complete mono-layer of fine particles. Thus, when drug particles are in close proximity to each other, they will experience both adhesion and cohesion forces, i.e. drug-carrier and drug-drug interactions. The overall effect might create a strong adhesion layer, reducing the propensity of the particles to detach and leading to the FPF decreasing. Eventually, the surface cavities are saturated with fines and with further increase in drug load, fines will start to adhere to the enveloped carrier surfaces, i.e. a blend state 2a.Since Inhalac 70 has a complex particle morphology it is possible that that the transition from S1 to S2a is not a distinct process but rather a diffuse transition where the adsorption of single particles to flat enveloped carrier surfaces (S2a) co-exists with the completion of particle attachment into carrier cavities.

When the drug concentration continues to increase even further, multi-layers of particles will be formed, and the adhesion layer will be more porous and thicker, i.e. a blend state 2b. As the separation distance between the drug and carrier surface increases, the drug particles will experience reduced adhesion and cohesion forces due to a more loosely packed structure. The consequence will be an increased FPF_{max}. In analogy, the blend state 1 may also be sub-divided into a S1a and a S1b state, i.e. when surface cavities are nearly completely filled the outermost particle layers may be more loosely packed and from which particles detach more easily. Since the concentration range of S1 is low such an effect is in practice difficult to demonstrate.

As discussed above, at low particle concentrations, a significant fraction of particles may exist as singular adhered particles, especially for the low particle concentrations positioned in S1 or S2a, and these particles may also detach as single particles. Inertial detachment, due to collisions between different particles, is considered to be an important detachment mechanism, with inertial forces that are strongly dependent on mass (Kassinos et al., page 125-126). Thus, if this mechanism is dominant, it is likely that the larger particles within a population are predominantly liberated and dispersed, while the smaller particles remain adhered to the lactose during dose withdrawal. As multi-layers are formed in the latter parts of S1 and S2a, involving drug-drug bonding forces, it might become harder for individual particles to detach. Instead, micro-agglomerates may detach, including both larger and smaller particles, which subsequently are disintegrated, with the consequence that MMAD decreases. Alternatively, other detachment mechanisms might be involved, such as the scraping off of micro-agglomerates due to shearing forces. When the S2b phase is entered, a thicker and more irregularly packed adhesion layer is formed, facilitating the tendency to liberate increasingly larger micro-agglomerates that are too large to be completely disintegrated, resulting in an increased MMAD with drug load.

The pressure drop had a clear effect on the drug dispersion, as assessed by the FPF and MMAD (Figure 7). In an approximate generalisation, the pressure drop shifted the relationship between drug load and FPF or MMAD along the x-axis, i.e. towards higher FPF and lower MMAD. Thus, the similarity of the FPF-drug concentration relationships at different pressure drops indicate that the structure of the adhesive mixtures is the underlying cause for the wave-line response. The effect of pressure drop on dispersion, namely pressure drop sensitivity (Figure 10), was dependent on the

drug load, and an increased drug load increased the pressure drop sensitivity. However, this relationship showed a similar complexity as the FPF-drug load relationships, indicating that the blend state, i.e. the position of the drug particles on the carrier surface and the volume and structure of the adhesion layer, had a major role in the sensitivity to pressure drop. The dispersion rate, calculated by Eq. 3, represents another indication of how the formation of fine particles depends on the pressure drop, i.e. a pressure drop sensitivity parameter based on the complete FPF-ΔP profile (Figure 11). Additionally, k_d generally decreased with an increase in the drug load, albeit at a declining rate. Thus, the aerosolisation became more dependent on the pressure drop through the inhaler with increased drug load. This gradual change in pressure drop dependency might be caused by a change in the dominating detachment mechanism involved in aerosolisation. As discussed above, a gradual change from inertial detachment, due to impaction, to erosion detachment due to shearing forces, might occur when an enveloped adhesion layer forms.

There are several potential mechanisms by which drug particles can detach from the carrier. Such mechanisms can be categorised into two groups: particle-fluid interactions and particle-solid (particle or wall) interactions (Donovan and Smyth, 2010). The first group involves phenomena such as blowing off, lifting and centrifugation, while the second group involves repelling due to impaction and scraping off due to shearing. We cannot provide any evidence regarding which detachment mechanisms dominate the drug liberation process for the systems under investigation here. However, since the formation of a gradually thicker adhesion layer was associated with a change in both FPF_{max} and $MMAD_{min,}$ it is plausible that there is a change in the dominating detachment mechanism with the drug load. When drug particles are shielded from direct contact with other surfaces (S1), a reasonable liberation mechanism is that the particles are knocked off by inertia due to impaction. When particles are located on the enveloped carrier surface (S2), the drug particles will get direct contact with other surfaces during sliding, which might scrape off particles from the outermost adhesion layer or liberate particles through interaction with flowing air. This is consistent with an earlier proposal of an erosion liberation mechanism for this type of formulation (Rudén et al., 2022). The erosion mechanism depends upon the intensity of the shearing process, which increases with the pressure drop.

4.4. Aerosolisation propensity of Inhalac 230

In addition, for Inhalac 230, a variable and wave-like progression of the FPF-drug load and the MMAD-drug load relationships was obtained without a consistent trend towards increased or decreased FPF or MMAD (Figure 7). However, the increase in pressure drop not only shifted the positions of these relationships but also changed their progression, complicating the interpretation of the data. However, changes in the direction of the relationships occurred at similar drug concentrations across all pressure drops, i.e. at approximately 2 and 4%. Since self-agglomerates of API were observed in mixtures already at the two highest drug loads, which indicates the existence of blend state 3 already at low drug loads, the FPF-drug load relationships corresponded to only one region (up to about a SCR of 1) and of two drug load phases. In Figure 8, the FPF is plotted as a function of SCR up to a SCR of 1 at two pressure drops for both carriers. The wave-like response was similar for both carriers, albeit slightly shifted along the x-axis. However, the same reasoning, involving different blends states as for Inhalac 70, can explain these relationships. Due to the low concentration range of blend state 2, the transition point between blend state 2a and 2b is difficult to identify.

4.5. Effect of carrier properties on the aerosolisation propensity

The aerosolisation propensity differed between mixtures using the two carriers. Specifically, Inhalac 230 tended to have higher FPF_{max} and k_d values, with a larger $MMAD_{min}$ (Figure 11). Moreover, the loading capacity, i.e. the approximate drug load at which free self-agglomerates of drugs appeared (i.e. S3), was significantly lower for Inhalac 230 than for Inhalac 70, and the duration of the S2 state was markedly lower. The fact that the highest FPF_{max} values of Inhalac 70 were obtained for mixtures considered to be in S3 state indicates that these agglomerates might disperse during the actuation of the inhaler. Nevertheless, a segregated mixture should be avoided due to the risk of increased variability in the delivered dose (Thalberg et al., 2012). In contrast, for Inhalac 230, the presence of self-agglomerates (occurring at a SCR of 0.75) led to a decrease in the FPF_{max}. One reason for this might be that the larger size of the Inhalac 70 particles (relative to the Inhalac 230 particles) results in higher collision forces, not only during blending but also during inhalation, aiding the breakup of self-agglomerates.

In a previous study (Rudén et al., 2018), it was found that larger carrier particles had a higher loading capacity compared to smaller carriers, which is consistent with the findings in this study. The increased mass will give higher collision forces during mixing, sometimes referred to as higher press-on forces, affecting the distribution of drug across the carrier surface (Grasmeijer et al., 2013a). The drug particles may, thus, be smeared out more effectively during mixing and form a more compact and cohesive adhesion layer. Moreover, Inhalac 70 particles seemed to have a more irregular surface texture, which may also affect the adhesion between drug particles and the carrier surface (Flament et al., 2004).

Grasmeijer et al. (2013b) studied the effect of drug load, up to 4%, on the drug detachment for binary adhesive mixtures prepared by mixing for 10 mins using a lactose carrier. For one of the two drugs, fluticasone, the fraction of drug detached (%) vs drug load relationships showed a "wave like" response. For the other drug, salmeterol, a variable detachment with drug load was observed, but without the initial reduction in detachment at low drug loads, which could be associated with blend state 1. This indicates that differences in drug properties, such as particle size and surface energy, in combination with the carrier morphology and the mixing conditions, might affect the expression of blend states and the structure of the adhesive layer. Such differences will subsequently affect the FPF-drug load relationship.

5. Conclusion

Carrier-drug adhesive blends are seemingly simple powder systems that however have complicated properties. To further our understanding of the fundamentals controlling the performance of adhesive blends, improved knowledge of the influence of micro-structural features and particle configurations of the mixture is important. We here found that the dispersibility of the mixtures showed a complex, wave-like dependency of drug load that was repeated at different pressure drops albeit with more amplified variations with increased pressure drop. We propose that this response could be linked to the evolution of mixture structure and that up to five blend states, denoted *1a*, *1b*, *2a*, *2b* and *3*, can explain the response. States *1* and *2* refers to the main localization of drug particles on the carrier, i.e. in surface cavities or on enveloped surfaces respectively, and state *a* and *b* refers to the structure of the adhesion layer, i.e. *a* and *b* refers to monolayer and multilayer adhesion respectively. In both state *1* and *2*, the

dispersibility of the mixtures showed a u-shaped relationship to drug load. We also found that the dispersibility and the rate of dispersion (pressure drop sensitivity) related to each other in a non-linear and inverted manner and both these dispersion properties seemed to be linked to the blend state. It was finally found that the size and morphology of the carrier affected markedly the mixture dispersibility. Since both carriers consisted of crystalline lactose and consequently had similar cohesion-adhesion properties in relation to the drug, it can be concluded that the mass and morphology of the single carrier particles are critical for the evolution of mixture structure and the subsequent aerosolisation performance.

We conclude that the blend state concept is one approach by which structure-performance relationships of adhesive mixtures can be rationalized. In order to better understand the importance of the blend state there is a need to investigate also the relationship between blend state and manufacturing properties of adhesive mixtures, for example by flow and rheological properties. Such knowledge can be used as a means to understand optimal drug load regions suitable for both manufacturing and use of an inhalation powder. Other potential applications of concepts such as the blend state model in the formulation of adhesive mixtures are: Firstly, to aid the selection of carrier properties and the engineering of optimal carrier morphology. Secondly, since adhesive mixtures are dynamic systems dependent on the mixing conditions (intensity and time), to facilitate interpretation of relationships between mixing conditions and mixture performance. Thirdly, since mixture structure may depend on the interaction between the particles of the blend (sometimes expressed in terms of a cohesive – adhesive balance), to facilitate interpretation of the effect of modulated interparticle interactions on mixture performance.

We also conclude that the performance of the adhesive mixtures is affected by the blend state and the drug-drug and drug-carrier interactions of the adhesive layer in combination with the mechanism of detachment. Thus, ultimately, a fundamental understanding of mixture structure may open up for the prediction of adhesive blend performance by identifying and deriving indications of adhesion layer structure and strength, including factors such as the thickness, the rugosity, the packing density and the interparticle bond forces of the adhesive layer.

Acknowledgements

This study is a part of the science programme of the Swedish Drug Delivery Centre (SweDeliver), and financial support from VINNOVA (Dnr 2019-00048) is gratefully acknowledged. The authors are also grateful to Dr Lucia Lazorova, for preparing the SEM images and for assistance in the preparation of figures. We acknowledge Myfab Uppsala, which is a national research infrastructure funded by the Swedish Research Council (2019-00207), for providing experimental facilities.

References

Alderborn, G., Duberg, M., Nyström, C., 1985. Studies on direct compression of tablets X. Measurement of tablet surface area by permeametry. Powder Technology. 41, 49-56. https://doi.org/10.1016/0032-5910(85)85074-9

Buttini, F., Brambilla, G., Copelli, D., Sisti, V., Balducci, AG., Bettini, R., Pasquali, I., 2016. Effect of Flow Rate on In Vitro Aerodynamic Performance of NEXThaler(®) in Comparison with Diskus(®) and Turbohaler(®) Dry Powder Inhalers. Journal of Aerosol Medicine and Pulmonary Drug Delivery. 29, 167-78. https://doi.org/10.1089/jamp.2015.1220

Clark, AR., Weers, JG., Dhand, R., 2020. The Confusing World of Dry Powder Inhalers: It Is All About Inspiratory Pressures, Not Inspiratory Flow Rates. Journal of Aerosol Medicine and Pulmonary Drug Delivery. 33, 1–11. https://www.liebertpub.com/doi/10.1089/jamp.2019.1556

Demoly, P., Hagedoorn, P., de Boer, A., Frijlink, H., 2014. The clinical relevance of dry powder inhaler performance for drug delivery. Respiratory Medicine. 108, 1195-1203. https://doi.org/10.1016/j.rmed.2014.05.009

Donovan, MJ., Smyth., HD., 2010. Influence of size and surface roughness of large lactose carrier particles in dry powder inhaler formulations. International Journal of Pharmaceutics. 402, 1-9. https://doi.org/10.1016/j.ijpharm.2010.08.045

Elsayed, MMA., Shalash, AO., 2018. Modeling the performance of carrier-based dry powder inhalation formulations: Where are we, and how to get there? Journal of Controlled Release. 279, 251-261. https://doi.org/10.1016/j.jconrel.2018.03.020

Eriksson, M., Nyström, C., Alderborn, G., 1993.The use of air permeametry for the assessment of external surface area and sphericity of pelletized granules. International Journal of Pharmaceutics. 99, 197-207. https://doi.org/10.1016/0378-5173(93)90362-J

Farizhandi, A., Pacławski, A., Szlęk, J., Mendyk, A., Shao, Y-H., Lau, R. 2019. Evaluation of carrier size and surface morphology in carrier-based dry powder inhalation by surrogate modeling. Chemical Engineering Science. 193, 144-155. https://doi.org/10.1016/j.ces.2018.09.007

Flament, M-P., Leterme, P., Gayot, A., 2004. The influence of carrier roughness on adhesion, content uniformity and the *in vitro* deposition of terbutaline sulphate from dry powder inhalers. International Journal of Pharmaceutics. 275, 201–209. https://doi.org/10.1016/j.ijpharm.2004.02.002

Grasmeijer, F., Hagedoorn, P., Frijlink, HW., de Boer, HA., 2013a. Mixing time effects on the dispersion performance of adhesive mixtures for inhalation. PLoS One. 8 (7), 1-18. https://doi.org/10.1371/journal.pone.0069263

Grasmeijer, F., Hagedoorn, P., Frijlink, HW., de Boer, AH. 2013b. Drug content effects on the dispersion performance of adhesive mixtures for inhalation. PLoS One.8 (8), 1-12. https://doi.org/10.1371/journal.pone.0071339

Grasmeijer, F., de Boer, AH., 2014. The dispersion behavior of dry powder inhalation formulations cannot be assessed at a single inhalation flow rate. International Journal of Pharmaceutics. 465, 165–168. https://doi.org/10.1371/journal.pone.0071339

Grasmeijer, F., Grasmeijer, N., Hagedoorn, P., Frijlink, HW., Haaije de Boer, A., 2015. Recent advances in the fundamental understanding of adhesive mixtures for inhalation. Current Pharmaceutical Design. 21, 5900-5914. https://doi.org/10.2174/1381612821666151008124622

Hertel, M., Schwarz, E., Kobler, M., Hauptstein, S., Steckel, H., Scherließ, R., 2018. Powder flow analysis: A simple method to indicate the ideal amount of lactose fines in dry powder

inhaler formulations. International Journal of Pharmaceutics, 535, 59-67. https://doi.org/10.1016/j.ijpharm.2017.10.052

Hoppentocht, M., Hagedoorn, P., Frijlink, HW., de Boer, AH., 2014. Technological and practical challenges of dry powder inhalers and formulations. Advanced Drug Delivery Reviews. 75, 18-31. https://doi.org/10.1016/j.addr.2014.04.004

Jaffari, S., Forbes, B., Collins, E., Barlow, DJ., Martin, GP., Murnane, D., 2013. Rapid characterization of the inherent dispersibility of respirable powders using dry dispersion laser diffraction. International Journal of Pharmaceutics. 447,124-131. https://doi.org/10.1016%2Fj.ijpharm.2013.02.034

Jones, MD., Buckton, G., 2016. Comparison of the cohesion-adhesion balance approach to colloidal probe atomic force microscopy and the measurement of Hansen partial solubility parameters by inverse gas chromatography for the prediction of dry powder inhalation performance. International Journal of Pharmaceutics. 509, 419-430. https://doi.org/10.1016/j.ijpharm.2016.06.002

Kassinos, S., Bäckman, P., Conway, J., Hickey, A., (2021) Inhaled Medicines: Optimizing Development through Integration of In Silico, In Vitro and In Vivo Approaches, first ed. Academic Press, London, UK.

Mehta, P., 2018. Imagine the superiority of dry powder inhalers from carrier engineering. Journal of Drug Delivery. Article ID: 5635010. https://doi.org/10.1155/2018/5635010

Nguyen, D., Rasmuson, A., Niklasson, B., Thalberg, K., 2015. Mechanistic time scales in adhesive mixing investigated by dry particle sizing. European Journal of Pharmaceutical Sciences. 69, 19-25. https://doi.org/10.1016/j.ejps.2014.12.016

Nguyen, D., Remmelgas, J., Björn, IN., van Wachem, B., Thalberg, K., 2018. Towards quantitative prediction of the performance of dry powder inhalers by multi-scale simulations and experiments. International Journal of Pharmaceutics. 547, 31–43. https://doi.org/10.1016/j.ijpharm.2018.05.047

Rudén, J., Frenning, G., Bramer, T., Thalberg, K., Alderborn, G., 2018. Relationships between surface coverage ratio and powder mechanics of binary adhesive mixtures for dry powder inhalers. International Journal of Pharmaceutics. 541, 143-156. https://doi.org/10.1016/j.ijpharm.2018.02.017

Rudén, J., Frenning, G., Bramer, T., Thalberg K, An, J., Alderborn, G., 2019. Linking carrier morphology to the powder mechanics of adhesive mixtures for dry powder inhalers via a blend-state model. International Journal of Pharmaceutics. 561, 148–160. https://doi.org/10.1016/j.ijpharm.2019.02.038

Rudén, J., Frenning, G., Bramer, T., Thalberg, K., Alderborn, G., 2021. On the relationship between blend state and dispersibility of adhesive mixtures containing active pharmaceutical ingredients. International Journal of Pharmaceutics: X. 3, 1-14. https://doi.org/10.1016/j.ijpx.2020.100069

Rudén, J., Frenning, G., Bramer, T., Thalberg, K., Alderborn, G., 2022. Effect of pressure drop on the in vitro dispersion of adhesive mixtures of different blend states for inhalation. International Journal of Pharmaceutics. 617, 1-12. https://doi.org/10.1016/j.ijpharm.2022.121590

Sibum, I., Hagedoorn, P., de Boer, AH, Frijlink, HW., Grasmeijer, F., 2018. Challenges for pulmonary delivery of high powder doses. International Journal of Pharmaceutics. 548, 325-336. https://doi.org/10.1016/j.ijpharm.2018.07.008

Thalberg, K., Berg, E. Fransson, M. 2012. Modeling dispersion of dry powders for inhalation. The concepts of total fines, cohesive energy and interaction parameters. International Journal of Pharmaceutics. 427, 224-233. https://doi.org/10.1016/j.ijpharm.2012.02.009

Thalberg, K., Åslund, S., Skogevall, M., Andersson, P., 2016. Dispersibility of lactose fines as compared to API in dry powders for inhalation. International Journal of Pharmaceutics. 504, 27-38. https://doi.org/10.1016/j.ijpharm.2016.03.004

Yeung, S., Traini, D., Tweedie, A., Lewis, D., Church T, Young, PM., 2018. Limitations of high dose carrier-based formulations. International Journal of Pharmaceutics. 544, 141-152. https://doi.org/10.1016/j.ijpharm.2018.04.012

Yeung, S., Traini, D., Tweedie, A., Lewis, D., Church, T., Young, PM., 2019. Assessing aerosol performance of a dry powder carrier formulation with increasing doses using a novel inhaler. AAPS PharmSciTech. 20, 1-12. https://doi.org/10.1208/s12249-019-1302-6

Young, P., Edge, S., Traini, D., Jones, M., Price, R., El-Sabawi, D., Urry, U., Smith, C., 2005. The influence of dose on the performance of dry powder inhalation systems. International Journal of Pharmaceutics. 296, 26-33. https://doi.org/10.1016/j.ijpharm.2005.02.004

Young, P., Wood, O., Ooi, J., Traini, D., 2011. The influence of drug loading on formulation structure and aerosol performance in carrier based dry powder inhalers. International Journal of Pharmaceutics. 416, 129-135. https://doi.org/10.1016/j.ijpharm.2011.06.020

Zeng, XM., Martin, GP., Marriott C., Pritchard, J., 2000. The influence of crystallization conditions on the morphology of lactose intended for use as a carrier for dry powder aerosols. Journal of Pharmacy and Pharmacology. 52, 633-643. https://doi.org/10.1211/0022357001774462

Zellnitz, S., Pinto, JT., Brunsteiner, M., Schroettner, H., Khinast, J., Paudel, A., 2019. Tribo-Charging Behavior of Inhalable Mannitol Blends with Salbutamol Sulphate. Pharmaceutical Research, an official journal of the American Association of Pharmaceutical Scientists. 36, 1-11. https://doi.org/10.1007/s11095-019-2612-9

Zhu, Q., Gou, D., Li, L., Chan, H., Yang, R., 2022. Numerical investigation of powder dispersion mechanisms in Turbuhaler and the contact electrification effect. Advanced Powder Technology. 33, 1-11. https://doi.org/10.1016/j.apt.2022.103839

Table legends

Table 1. Some particle properties of budesonide and carriers (Inhalac 70 and Inhalac 230). Reported values are the mean, with standard deviations within brackets, from three separate measurements of the respective property.

Table 2. Surface coverage ratio, concentration, nominal and measured drug dose and blend homogeneity (expressed as relative standard deviation, RSD) of all adhesive mixtures.

Figure legends

Fig. 1. Effect of pressure drop (ΔP 0.5-4 kPa) on cumulative aerodynamic particle diameter distributions for the fraction of drug deposited in the impactor stages for adhesive mixtures of two concentrations for each carrier (left panel Inhalac 70, right panel Inhalac 230). The cumulative particle diameter distribution for the drug determined by LS (laser scattering) is included as a reference. Mean values and standard deviations (n=3).

Fig. 2. Scanning electron microscope images of budesonide (A), Inhalac 70 (B) and Inhalac 230 (C).

Fig. 3. Scanning electron microscope images of some of the adhesive mixtures for the two carriers representing different theoretical surface coverage ratio (SCR). (A) Inhalac 70, SCR 0.5 (1.00% Budesonide); (B) Inhalac 70, SCR 3 (6.06% Budesonide); (C) Inhalac 70, SCR 5 (10.10% Budesonide); (D) Inhalac 230, SCR 0.25 (1.19% Budesonide); (E) Inhalac 230, SCR 0.5 (2.38% Budesonide); (F) Inhalac 230, SCR 0.75 (3.78% Budesonide).

Fig. 4. Light microscope images of adhesive mixtures for the two carriers of high theoretical surface coverage ratio (SCR) showing presence of large agglomerates. (A): Inhalac 70, SCR 5 (10.10% Budesonide); (B) Inhalac 230, SCR 0.75 (3.58% Budesonide). Images were taken using a magnification of 1 x.

Fig. 5. The effect of pressure drop (ΔP 0.5-4 kPa) on the relationship between nominal dose (from homogeneity analysis) and emitted and retained dose of mixtures of Inhalac 70 (left graph) and Inhalac 230 (right graph). Mean values (n=3) and standard deviations.

Fig. 6. Fraction of emitted dose (mean values and standard deviations, n=3) deposited in the main parts of the impactor (induction port/throat, pre-separator and impactor stages), dependent on the pressure drop and blend concentration of all adhesive mixtures. Each bar colour represents one drug concentration, increasing from left to right along the x-axis. Upper panel: Mixtures of Inhalac 70. Lower panel: Mixtures of Inhalac 230.

Fig. 7. Effect of drug concentration on fine particle dose (left graphs), fine particle fraction (middle graphs) and mass median aerodynamic diameter (right graphs) after inhaler actuation at different pressure drops (ΔP 0.5-4 kPa). Mean values and standard deviations (n=3). Upper panel: Mixtures of Inhalac 70. Lower panel: Mixtures of Inhalac 230.

Fig. 8. Effect of SCR on FPF of mixtures of Inhalac 70 (squares) and Inhalac 230 (circles), SCR ranging up to 1. Red colour representing PD 1 kPa and blue colour representing PD 4 kPa. Mean values and standard deviations (n=3).

Fig. 9. Effect of drug concentration on the dispersibility of all adhesive mixtures of Inhalac 70 (circles) and Inhalac 230 (squares). Left graph: Maximum fine particle fraction calculated by eq. 3; Right graph: Minimum mass median aerodynamic diameter calculated by eq. 7.

Fig. 10. Effect of drug concentration on the pressure drop sensitivity of all adhesive mixtures of Inhalac 70 (circles) and Inhalac 230 (squares). Left graph: Calculated by eq. 5 using fine particle fraction; Right graph: Calculated by eq. 6 using mass median aerodynamic diameter

Fig. 11. Left graph: Effect of drug concentration on the dispersion rate constant calculated by eq. 3 of all adhesive mixtures of Inhalac 70 (circles) and Inhalac 230 (squares). Right graph: Relationship between dispersibility and rate of dispersion calculated by eq. 3 of all adhesive mixtures of Inhalac 70.

Table 1
Some particle properties of budesonide and carriers (Inhalac 70 and Inhalac 230). Reported values are the mean, with standard deviations within brackets, from three separate measurements of the respective property.

Material	Apparent particle density (gcm^{-3})	Particle weight specific surface area (cm^2g^{-1})	Median particle diameter (μm)	Span of particle diameter distribution (-)
Budesonide	1.27	45 530 (845)	2.1 (0.0)	1.58
Inhalac 70	1.54	280 (4.00)	247 (7.0)	0.74
Inhalac 230	1.54	661 (11.0)	104 (0.4)	1.00

Table 2
Surface coverage ratio, concentration, nominal and obtained drug dose and blend homogeneity (expressed as relative standard deviation, RSD) of all adhesive mixtures.

Carrier	SCR	% Budesonide	Target drug dose (μg)	Nominal drug dose (μg)	Homogeneity (RSD %)	Mass Budesonide/cm^2 carrier (μg)
Inhalac 70	0.25	0.50	75	81.26	5.14	19.45
	0.5	1.00	150	158.6	3.40	38.17
	0.75	1.51	225	245.2	2.20	59.35
	1	2.02	300	308.4	3.65	74.97
	2	4.04	600	585.6	3.16	145.1
	3	6.06	900	783.7	3.11	196.9
	4	8.08	1200	1160	5.01	299.3
	5	10.1	1500	1579	9.72	420.2
	7	14.1	2100	1576	7.90	419.3
Inhalac 230	0.17	0.80	120	127.0	7.79	12.92
	0.25	1.19	179	158.7	5.62	16.18
	0.5	2.38	357	348.2	3.63	35.95
	0.75	3.58	536	604.2	5.73	63.50
	1	4.77	714	697.5	8.73	75.78

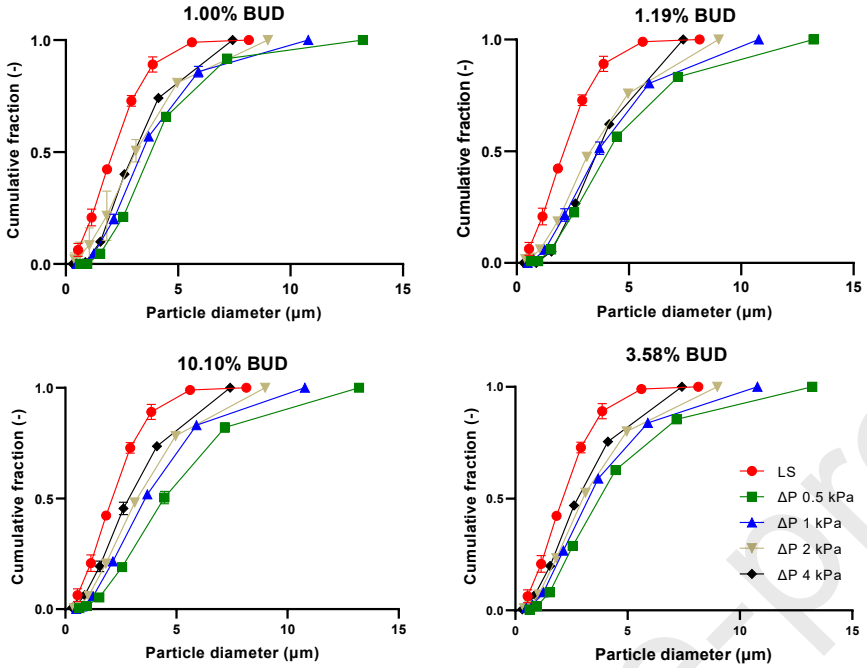

Fig. 1. Effect of pressure drop (ΔP 0.5-4 kPa) on cumulative aerodynamic particle diameter distributions for the fraction of drug deposited in the impactor stages for adhesive mixtures of two concentrations for each carrier (left panel Inhalac 70, right panel Inhalac 230). The cumulative particle diameter distribution for the drug determined by LS (laser scattering) is included as a reference. Mean values and standard deviations (n=3).

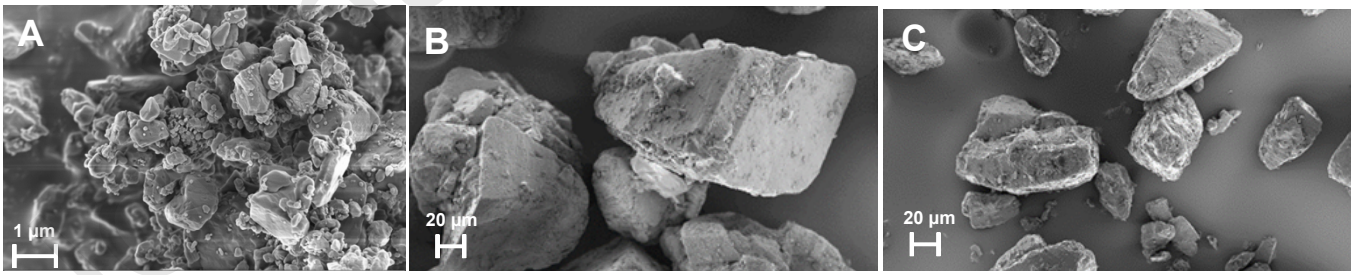

Fig. 2. Scanning electron microscope images of budesonide (A), Inhalac 70 (B) and Inhalac 230 (C).

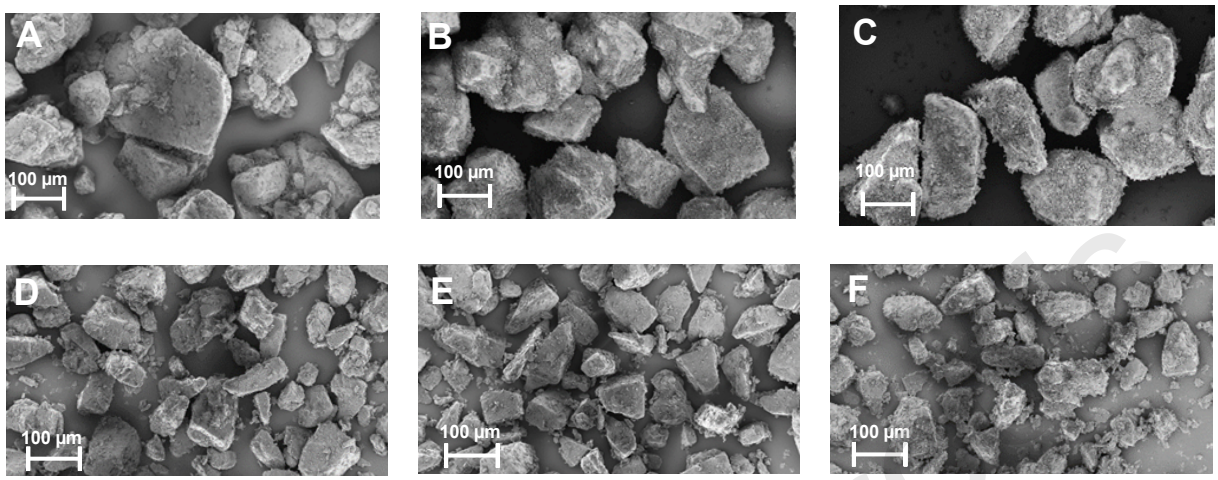

Fig. 3. Scanning electron microscope images of some of the adhesive mixtures for the two carriers representing different theoretical surface coverage ratio (SCR). (A) Inhalac 70, SCR 0.5 (1.00% Budesonide); (B) Inhalac 70, SCR 3 (6.06% Budesonide); (C) Inhalac 70, SCR 5 (10.10% Budesonide); (D) Inhalac 230, SCR 0.25 (1.19% Budesonide); (E) Inhalac 230, SCR 0.5 (2.38% Budesonide); (F) Inhalac 230, SCR 0.75 (3.78% Budesonide).

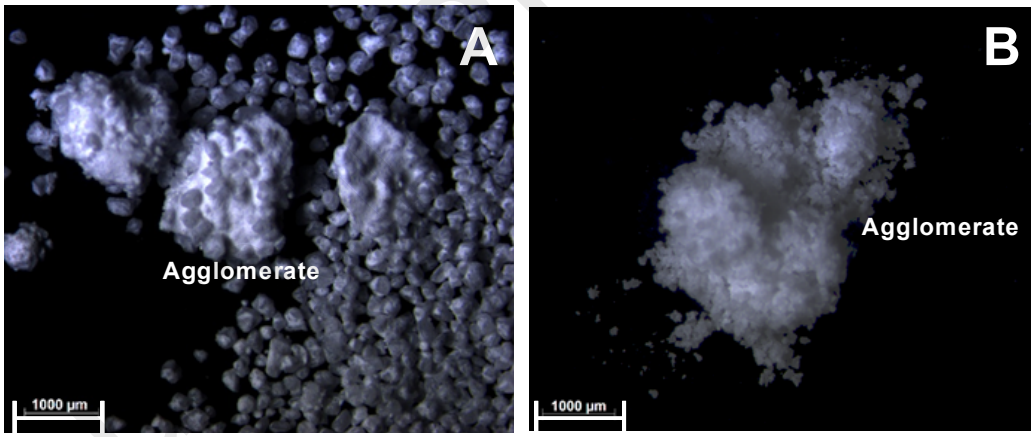

Fig. 4. Light microscope images of adhesive mixtures for the two carriers of high theoretical surface coverage ratio (SCR) showing presence of large agglomerates. (A): Inhalac 70, SCR 5 (10.10% Budesonide); (B) Inhalac 230, SCR 0.75 (3.58% Budesonide). Images were taken using a magnification of 1 x.

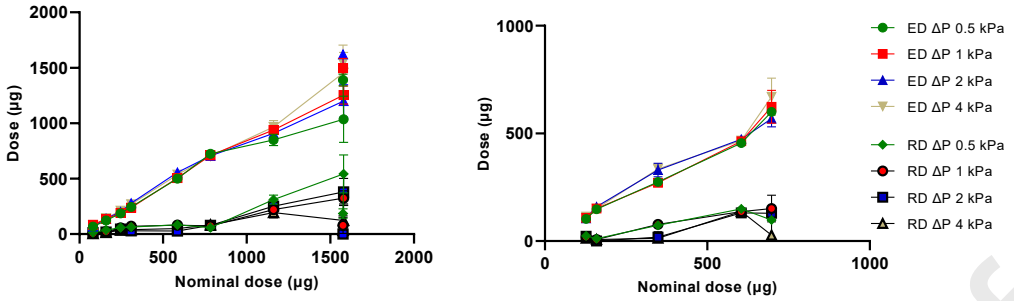

Fig. 5. The effect of pressure drop (ΔP 0.5-4 kPa) on the relationship between nominal dose (from homogeneity analysis) and emitted and retained dose of mixtures of Inhalac 70 (left graph) and Inhalac 230 (right graph). Mean values (n=3) and standard deviations.

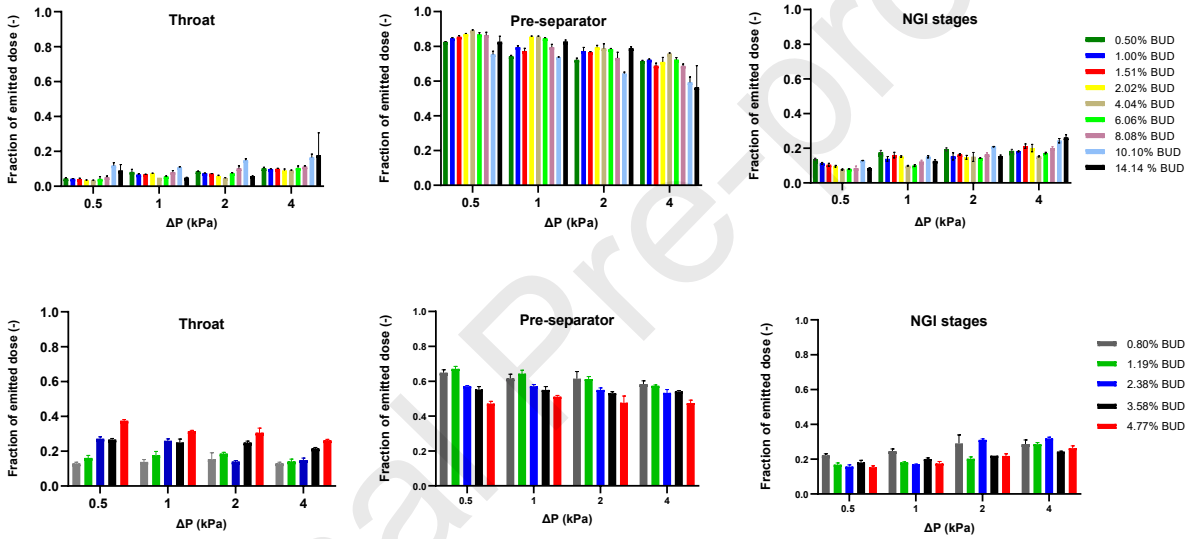

Fig. 6. Fraction of emitted dose (mean values and standard deviations, n=3) deposited in the main parts of the impactor (induction port/throat, pre-separator and impactor stages), dependent on the pressure drop and blend concentration of all adhesive mixtures. Each bar colour represents one drug concentration, increasing from left to right along the x-axis. Upper panel: Mixtures of Inhalac 70. Lower panel: Mixtures of Inhalac 230.

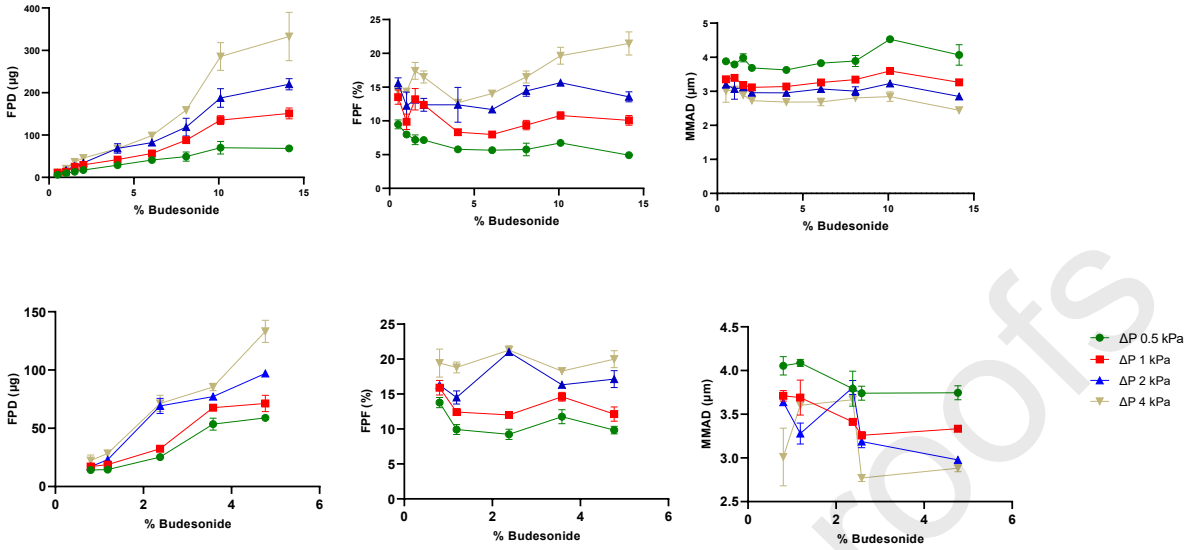

Fig. 7. Effect of drug concentration on fine particle dose (left graphs), fine particle fraction (middle graphs) and mass median aerodynamic diameter (right graphs) after inhaler actuation at different pressure drops (ΔP 0.5-4 kPa). Mean values and standard deviations (n=3). Upper panel: Mixtures of Inhalac 70. Lower panel: Mixtures of Inhalac 230.

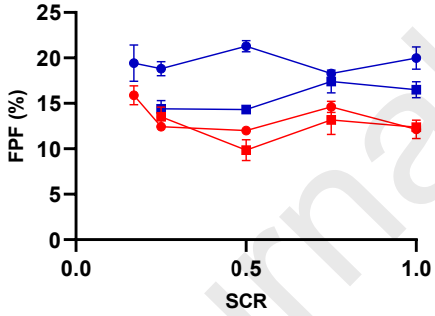

Fig. 8. Effect of SCR on FPF of mixtures of Inhalac 70 (squares) and Inhalac 230 (circles), SCR ranging up to 1. Red colour representing PD 1 kPa and blue colour representing PD 4 kPa. Mean values and standard deviations (n=3).

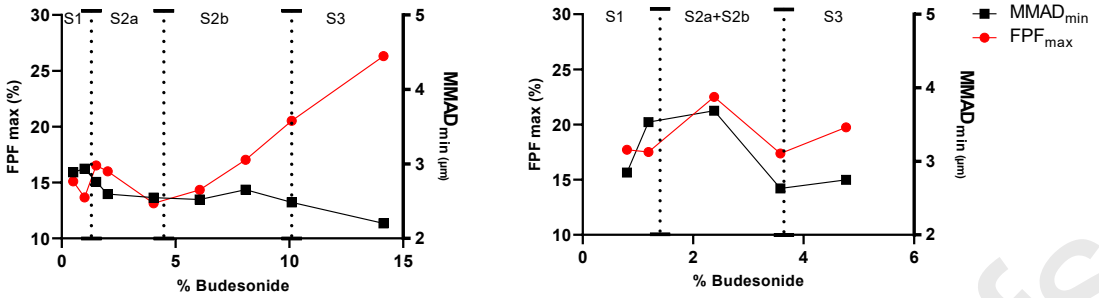

Fig. 9. Effect of drug concentration on the dispersibility of all adhesive mixtures of Inhalac 70 (circles) and Inhalac 230 (squares). Left graph: Maximum fine particle fraction calculated by eq. 3; Right graph: Minimum mass median aerodynamic diameter calculated by eq. 7.

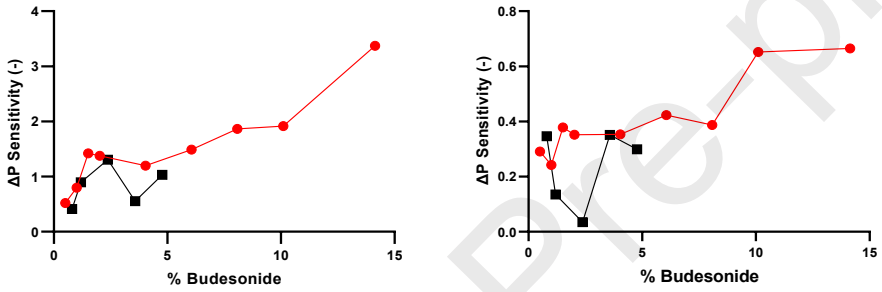

Fig. 10. Effect of drug concentration on the pressure drop sensitivity of all adhesive mixtures of Inhalac 70 (circles) and Inhalac 230 (squares). Left graph: Calculated by eq. 5 using fine particle fraction; Right graph: Calculated by eq. 6 using mass median aerodynamic diameter

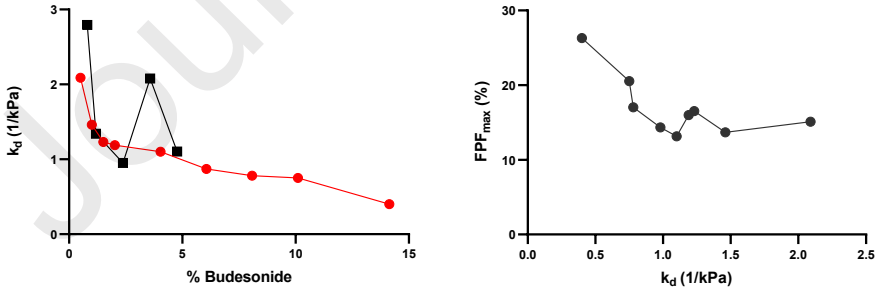

Fig. 11. Left graph: Effect of drug concentration on the dispersion rate constant calculated by eq. 3 of all adhesive mixtures of Inhalac 70 (circles) and Inhalac 230 (squares). Right graph: Relationship between dispersibility and rate of dispersion calculated by eq. 3 of all adhesive mixtures of Inhalac 70.

.

Declaration of interests

☐ The authors declare that they have no known competing financial interests or personal relationships that could have appeared to influence the work reported in this paper.

☒ The authors declare the following financial interests/personal relationships which may be considered as potential competing interests:

Anna Simonsson reports financial support was provided by Sweden's Innovation Agency. Tobias Bramer, Alex Wimbush reports financial support and equipment, drugs, or supplies were provided by AstraZeneca R&D Gothenburg. Tobias Bramer, Alex Wimbush reports a relationship with AstraZeneca R&D Gothenburg that includes: employment. Göran Alderborn is an editorial board member at Int. J. Pharm If there are other authors, they declare that they have no known competing financial interests or personal relationships that could have appeared to influence the work reported in this paper.

Graphical Abstract (for review)